Lieberman, R. S.; Smith, A. K.; Franke, S. J.; Vincent, Robert Alan; Isler, J. R.; Manson, A. H.; Meek, C. E.; Fraser, G. J.; Fahrutdinova, A.; Thayaparan, T.; Hocking, W.; MacDougall, J.; Nakamura, T.; Tsuda, T.
Comparison of mesospheric and lower thermospheric residual wind with High Resolution Doppler Imager, medium frequency, and meteor radar winds, Journal of Geophysical Research, 2000; 105(D22):27023-27035.

JOURNAL OF GEOPHYSICAL RESEARCH, VOL. 105, NO. D22, PAGES 27,023–27,035, NOVEMBER 27, 2000

Comparison of mesospheric and lower thermospheric residual wind with High Resolution Doppler Imager, medium frequency, and meteor radar winds

R. S. Lieberman,[1] A. K. Smith,[2] S. J. Franke,[3] R. A. Vincent,[4] J. R. Isler,[5,6] A. H. Manson,[7] C. E. Meek,[7] G. J. Fraser,[8] A. Fahrutdinova,[9] T. Thayaparan,[10,11] W. Hocking,[10] J. MacDougall,[10] T. Nakamura,[12] and T. Tsuda[12]

Abstract. The objective of this study is to compare observed mean meridional winds with those deduced from theory. The diabatic circulation is computed from High Resolution Dopper Imager (HRDI) mesospheric and lower thermospheric temperatures during January and July conditions. The meridional wind component is compared with HRDI Eulerian mean meridional winds near 95 km and with seasonal averages of meridional winds at a number of radar medium-frequency (MF) and meteor wind (MW) sites. The diabatic wind is directed from the summer toward the winter hemisphere. Peak values exceed 20 m s^{-1} and are observed at 105 km near 20° in the summer hemisphere. A secondary maximum of about 10 m s^{-1} is observed in the wintertime lower mesosphere during the July case. The diabatic wind is qualitatively consistent with HRDI 95-km mean meridional winds at latitudes equatorward of 50°. Time-averaged summertime radar winds are consistent with HRDI and diabatic winds between 50°S and 20°N. At winter midlatitudes, MF radar winds are directed oppositely to the diabatic wind, while one available MW measurement is directed with the diabatic wind. The zonal acceleration implied by the diabatic wind is about 150–200 m s^{-1} d^{-1} in the midlatitude summer lower thermosphere.

1. Introduction

Zonally averaged winds and temperatures in the mesosphere and lower thermosphere (MLT) are far from the state implied by radiative and photochemical equilibrium [*Leovy*, 1964]. It is generally accepted that the MLT zonal mean wind is maintained largely through forcing by nonconservative eddies. The eddies drive a "residual" mean meridional circulation which results in net adiabatic heating that prevents the atmosphere from relaxing to a purely radiatively controlled state. The residual vertical wind is the component of the Eulerian (or longitudinal) mean vertical wind whose advection by the basic state static stability is not canceled by the meridional convergence of the planetary wave heat flux. The residual meridional wind is defined from the continuity requirement for the residual mean circulation and is equal to the difference between the Eulerian mean meridional wind and the vertical convergence of the meridional planetary wave heat flux [*Andrews et al.*, 1987].

The physical significance of the residual mean circulation is twofold. As shown by *Garcia* [1987], the circulation is the key mechanism for restoring geostrophic and hydrostatic balance in a wave-driven atmosphere. Moreover, *Dunkerton* [1978] has shown that for steady and conservative quasigeostrophic planetary waves, the residual (or diabatic) circulation is equivalent to the zonally averaged Lagrangian, or mass, motion. The residual circulation is therefore a powerful tool for quantifying the material, or transport wind. Direct calculation of the circulation requires a global network of wind and temperature observations that is sufficiently dense for resolving the zonal mean and planetary-scale waves and is precise enough to reliably determine planetary wave fluxes and their spatial gradients. In practice, the residual circulation is generally diagnosed from observed and theoretical diabatic heating rates [*Solomon et al.*, 1986;

[1] Colorado Research Associates Division, Northwest Research Associates, Inc., Boulder.

[2] National Center for Atmospheric Research, Boulder, Colorado.

[3] Department of Electrical and Computer Engineering, University of Illinois, Urbana.

[4] Department of Physics and Mathematical Sciences, University of Adelaide, Adelaide, Australia.

[5] Laboratory for Space Physics, University of Colorado, Boulder.

[6] Now at Department of Physics, Wagner College, Staten Island, New York.

[7] Institute of Space and Atmospheric Studies, University of Saskatchewan, Saskatoon, Saskatchewan, Canada.

[8] Department of Physics and Astronomy, University of Canterbury, Christchurch, New Zealand.

[9] Physics Department, Kazan State University, Kazan, Russia.

[10] Department of Electrical Engineering, University of Western Ontario, London, Ontario, Canada.

[11] Now at Defense Research Establishment, Ottawa, Ottawa, Ontario, Canada.

[12] Radio Atmospheric Science Center, Uji, Kyoto, Japan.

Paper number 2000JD900363.
0148-0227/00/2000JD900363$09.00

Shine, 1989; *Huang and Smith,* 1991] or modeled using wave-drag parameterizations [*Garcia and Solomon,* 1985; *Zhu et al.,* 1997].

Direct measurements of seasonally averaged Eulerian mean meridional winds have been carried out with satellite and with medium-frequency (MF) and meteor wind (MW) radar winds. When averaged over periods long enough to remove transient components, MF or MW radar winds represent the climatological Eulerian mean wind plus stationary wave components. *Manson et al.* [1991] examined perturbation winds derived from the Committee on Space Programs and Research (COSPAR) International Reference Atmosphere (CIRA)-86 climatology, and monthly averaged meridional winds at a number of MF sites. Amplitudes of CIRA-86 planetary waves were very weak during summertime. Monthly mean summertime radar meridional winds were of the order of 10–15 m s^{-1} and directed equatorward, or from the summer toward the winter pole. In the absence of stationary components in the CIRA wind climatology, these were interpreted by *Manson et al.* [1991] as the Eulerian mean meridional winds.

Lieberman et al. [1998] examined 60-day averages of zonally averaged UARS High Resolution Doppler Imager (HRDI) mean meridional winds near 95 km and compared these with radar winds at a number of sites. HRDI low and midlatitude solstice winds were generally directed from the summer hemisphere toward the winter hemisphere with magnitudes of about 10–15 m s^{-1}. HRDI meridional wind values were consistent with coincident summertime radar winds and with previous values reported by *Manson et al.* [1991], but the peak values are higher than the existing model estimates of residual winds [*Garcia and Solomon,* 1985; *Huang and Smith,* 1991].

The purpose of this study is to calculate MLT residual meridional winds from HRDI temperatures and to compare these with radar and HRDI winds. This exercise provides an important cross validation between ground- and satellite-based mean wind estimates and updates earlier residual meridional wind estimates that are based upon simpler radiative heating algorithms and CIRA-86 climatological inputs [*Huang and Smith,* 1991]. Our study also provides some validation of more recent two-dimensional models of the residual mean circulation incorporating revised radiative heating and gravity wave drag parameterizations [*Portmann,* 1994; *Zhu et al.,* 1997]. Section 2 describes wind and temperature observations and the model used to calculate the diabatic circulation. Diabatic meridional winds are compared with HRDI and radar winds in section 3. A discussion and summary appear in section 4.

2. Model and Input Fields

2.1. Residual Circulation Model

The residual circulation in the middle atmosphere can be computed from the transformed Eulerian mean thermodynamic and continuity equations. The spherical version of these equations in log-pressure coordinates is presented by *Andrews et al.* [1987] and is given by

$$\cos\phi^{-1}(\overline{v}^*\cos\phi)_y + \rho_0^{-1}(\rho_0\overline{w}^*)_z = 0 \quad (1)$$

$$\overline{\Theta}_t + \overline{v}^*\overline{\Theta}_y + \overline{w}^*\overline{\Theta}_z = e^{\kappa z/H}(\overline{Q}_r + \sigma) + \overline{Q}_{chem} + H_D - \rho_0^{-1}[\rho_0(\overline{v'\theta'}\overline{\Theta}_y/a\overline{\Theta}_z + \overline{w'\theta'})]_z \quad (2)$$

$$\int_{-\pi/2}^{\pi/2}\rho\overline{w}^*\cos\phi d\phi = 0. \quad (3)$$

$\overline{Q}_r$ and $\overline{Q}_{chem}$ in (2) represent the radiative and chemical heating rates. H_D is the turbulent heating due to breaking gravity waves, usually represented as a diffusion of the mean thermal field [*Schoeberl et al.,* 1983; *Huang and Smith,* 1991]. The quantity σ is a correction factor introduced in order to achieve the global mass balance requirement formulated in (3). Following *Shine* [1989] and *Huang and Smith* [1991], σ is specified as a function of altitude only. Here $\overline{v}^*$ and $\overline{w}^*$ are the residual meridional and vertical winds, respectively, and are related to their Eulerian counterparts $\overline{v}$ and $\overline{w}$ by

$$\overline{v}^* = \overline{v} - \rho_0^{-1}(\rho_0\overline{v'\theta'}/\Theta_{0z})_z \quad (4)$$

$$\overline{w}^* = \overline{w} + (\overline{v'\theta'}/\Theta_{0z})_y. \quad (5)$$

Several assumptions and simplifications are invoked before applying (1)–(3). Because monthly mean solstice conditions are considered, the time derivative of temperature is weak compared with the other terms in (2) and is disregarded. The meridional gradient of $\overline{\Theta}$ is assumed to be at least an order of magnitude weaker than the vertical gradient; thus the term on the right-hand side of (2) involving the ratio $\overline{\Theta}_y/\overline{\Theta}_z$ is neglected. The vertical heat flux divergence $(\rho_0^{-1}(\rho_0\overline{w'\theta'})_z)$ associated with extratropical planetary waves has been shown to be very weak in the middle atmosphere [*Hitchman and Leovy,* 1986] and disappears altogether under midlatitude quasi-geostrophic scaling [*Andrews et al.,* 1987]. The direct heating effects of quasi-geostrophic planetary waves are therefore not considered. Planetary-scale, vertically propagating equatorial waves such as Kelvin waves and tides can, however, transport heat efficiently in the vertical and may result in significant heat flux divergence in a region of strong dissipation. The possible contribution of the diurnal tides to the zonally averaged thermodynamics budget is discussed in the next section.

Gravity wave saturation affects the zonally averaged thermal budget through the wave heat flux convergence and generation of diffusive heating by turbulence (the H_D term). It has been further shown that the net effects of gravity wave heating depend upon the localization of the turbulence [*Fritts and Dunkerton,* 1985; *Coy and Fritts,* 1988; *Liu,* 2000]. *Strobel et al.* [1985] and *Strobel* [1989] considered the implications of observed mean wind accelerations and tracer transport for the globally averaged heating budget in the upper mesosphere that included gravity wave heating. They concluded that a Prandtl number of about 3 was required in their parameterizations of gravity wave drag and turbulent heating. This implies that the net heating by gravity

waves is quite weak. A similar conclusion was reached by *Gavrilov and Roble* [1994], who found that parameterized gravity wave dissipation was nearly balanced by turbulent heating near 100 km.

Huang and Smith [1991] examined the effects of parameterized gravity wave heat flux and turbulent diffusion on the residual circulation. Although the circulation itself was relatively insensitive to the effective Prandtl number, global mass balance requirements were more readily satisfied when a high Prandtl number (10 or larger) was specified. This result is consistent with studies that found weak net thermal effects of gravity waves upon the global mean thermodynamic budget. However, the issue of the Prandtl number is far from resolved, owing to the paucity of measurements of gravity wave heating [*Gardner and Yang,* 1998] and the difficulty in specifying turbulence localization parameters. In view of these uncertainties, we have elected to not include parameterized gravity wave heating in our model of the mean meridional circulation.

Calculation of the net radiative heating rate $\overline{Q}_r$ is carried out with the algorithm of *Zhu* [1994]. The algorithm determines solar UV heating rates by O_2 and O_3 from an updated *Strobel* [1978] parameterization. IR cooling rates are computed for the CO_2 15-μ band, the O_3 9.6-μ band,

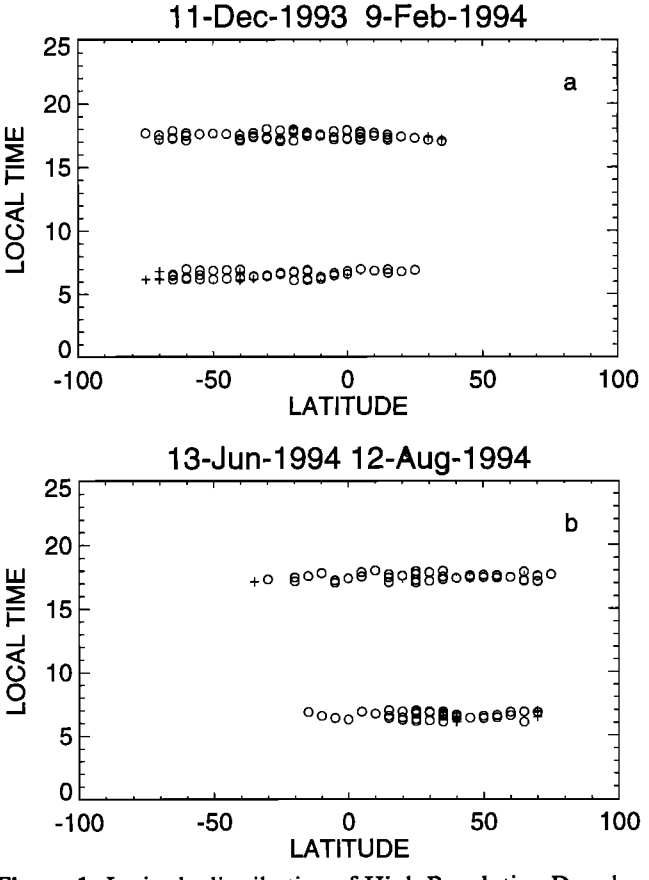

Figure 1. Latitude distribution of High Resolution Doppler Imager temperatures sampled at 0600 and 1700, used to construct Figure 2. a) Dots indicate December, circles indicate January, and plus signs indicate February. b) Dots indicate June, circles indicate July, and plus signs indicate August.

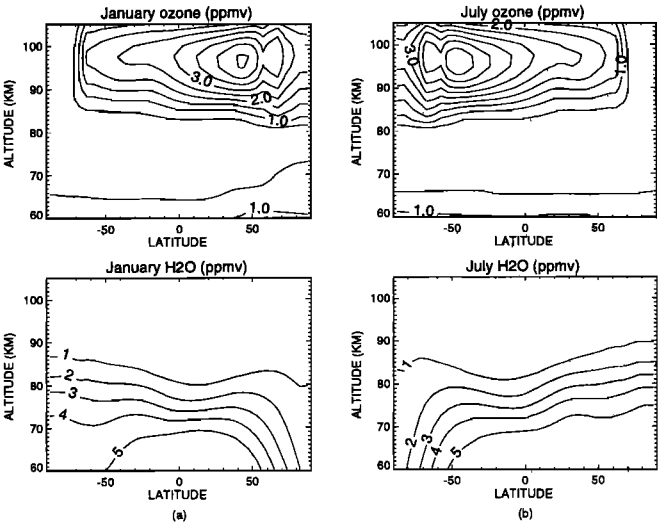

Figure 2. Ozone and water vapor mixing ratios in parts per million by volume (ppmv) representative of (a) January and (b) July conditions.

and the H_2O rotational lines and 6.3-μ band by interpolation of precomputed Curtis matrices which include non-local thermodynamic equilibrium source processes [*Zhu,* 1990]. Chemical heating $\overline{Q}_{chem}$ due to exothermic reactions involving oxygen and hydrogen [*Brasseur and Offerman,* 1986] is calculated in the Simulation Of Chemistry, Radiation, And Transport of Environmentally Important Species (SOCRATES) model, an updated version of the National Center for Atmospheric Research (NCAR) two-dimensional coupled dynamical-chemical middle atmosphere model [*Brasseur et al.,* 1990].

2.2. Input Parameters and Heating Fields

The residual circulation is computed for both July and January conditions. The tropospheric and stratospheric inputs to the net radiative heating rate $\overline{Q}_r$ are climatological values of ozone [*Keating and Pitts,* 1987], water vapor, and temperature. Above 80 km, mixing ratios from the SOCRATES model are used for water vapor and for ozone. HRDI seasonally averaged temperatures are used as input above 65 km. Two solstice-centered periods are represented: December 11, 1993 to February 9, 1994 and June 13 to August 12, 1994. These intervals are chosen because they are characterized by relatively wide HRDI data coverage in latitude (70°S to 30°N) and local time (about 12 hours). Because of the daytime-only sampling by HRDI over much of the 60- to 110-km range, migrating tidal signatures alias to the zonal mean and cannot generally be fully filtered from the long-term averages [*Morton et al.,* 1993; *Hays et al.,* 1994; *Ortland et al.,* 1998]. Tidal effects can, however, be somewhat mitigated by constructing temperature fields from measurements sampled nearly 12 hours apart [*Hitchman and Leovy,* 1985; *Lieberman,* 1999b]. The orbital precession of UARS implies that 12-hour differences in HRDI temperatures cannot generally be formed from measurements on the same day, or even within the same week or month. How-

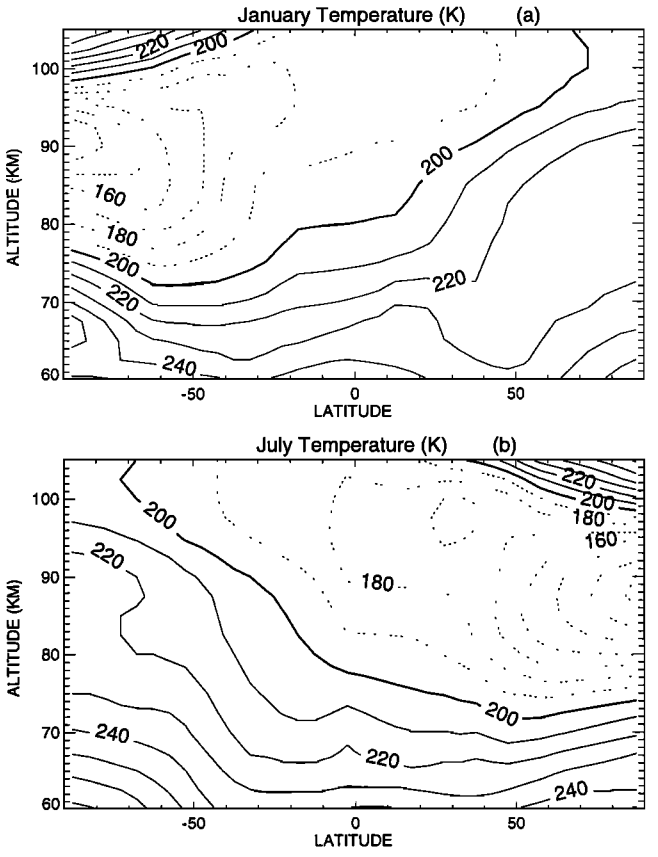

Figure 3. Zonal mean temperature inputs. Contour interval is 10 K, with dotted contours highlighting temperatures colder than 200 K. (a) January case. (b) July case.

ever, Figure 1 does indicate that the latitudinal coverage by HRDI at 0600 and 1700 is fairly broad, with measurements at both local times occurring nearly everywhere within the same calendar month (January and June) except at 70°S and 75°S between December and February. Accordingly, this study considers the average of HRDI zonal mean temperatures collected at 0600 and 1700 between December 11, 1993 and February 9, 1994, and from June 13 to August 12, 1994.

Global ozone and water vapor inputs are shown in Figure 2. Figure 3 shows the global temperature fields for both periods. HRDI temperatures are reported at 2.5-km intervals between 60 and 110 km and are binned in 5°-wide latitude bins. Below 65 km, HRDI temperatures were merged with climatological temperatures using 1–2–1 vertical smoothing at 65 km. Owing to diminished HRDI coverage in the winter hemisphere, climatological temperatures are also retained northward of 25°N for the December–February case and southward of 15°S for the June–August period. Poleward of 72° in the summer hemisphere, HRDI temperatures are linearly extrapolated to 87.5°, using the value of the meridional gradient at 72°. In order to weaken residual tidal contamination, HRDI temperatures in the 65- to 100-km range and between 20°N and 20°S are smoothed with a five-point boxcar algorithm.

Radiative and chemical heating rates for both seasons are shown in Figures 4–6. Solar heating peaks in the summer polar latitudes at the stratopause and in the lower thermosphere. This is due primarily to absorption by ozone in the stratosphere and molecular oxygen in the lower thermosphere. Chemical heating due to atomic oxygen recombination is most important in the winter lower thermosphere, reaching values of the order of the solar heating. The dominant cooling rate in the middle atmosphere is associated with the 15-μ band CO_2. The most striking feature is the contrast between the cooling rates in the summer and winter mesosphere. The net cooling rate maximum in the summer polar mesopause (Figure 6) is substantially stronger than reported in previous studies [*Zhu*, 1994; *Huang and Smith*, 1991] and may reflect the different zonally averaged temperature inputs. The vertical extent of the HRDI cold summer mesopause is narrower compared with the CIRA temperature input to the cooling schemes of *Dickinson* [1984], *Huang and Smith* [1991], and *Zhu* [1994], with temperatures at 100 km being warmer than CIRA by about 20K. The HRDI temperature structure is consistent with ground-based lidar climatologies showing the CIRA midlatitude temperatures at 100 km are about 5–10 K too cold [*Leblanc et al.*, 1998].

Inspection of the heating and cooling rates shown in Figures 4 and 5, respectively, clearly indicates that the diabatic heating algorithm used in this study produces strong net cooling at all latitudes above 100 km. As noted by *Zhu* [1994], a globally averaged downward diffusion of heat from the thermosphere is required to balance the global net diabatic cooling. Thermal input due to molecular heat conduction begins to be important above 100 km. The thermal conductivity coefficient was estimated using the formulation of *Banks and Kocharts* [1974] for an atmosphere with climatogical vertical distributions of N_2, O_2, and O. Heat conduction was quite weak near 100 km. Because HRDI temperature data do not extend far above 100 km, an accurate estimation of the vertical temperature gradient and the

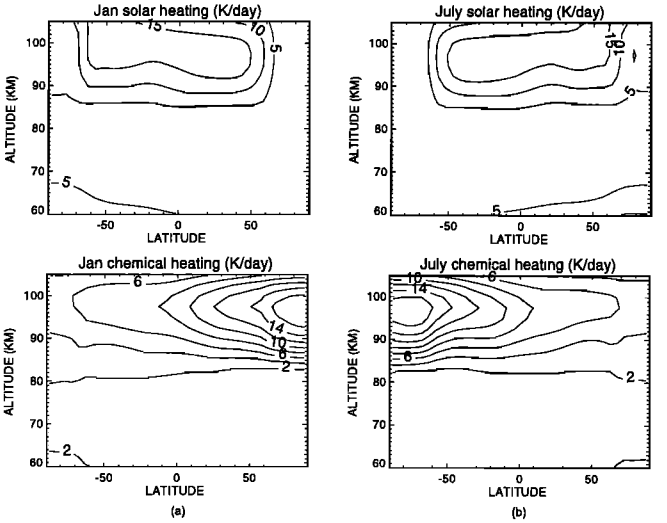

Figure 4. Solar and chemical heating rates for (a) January and (b) and July. Units are K d^{-1}.

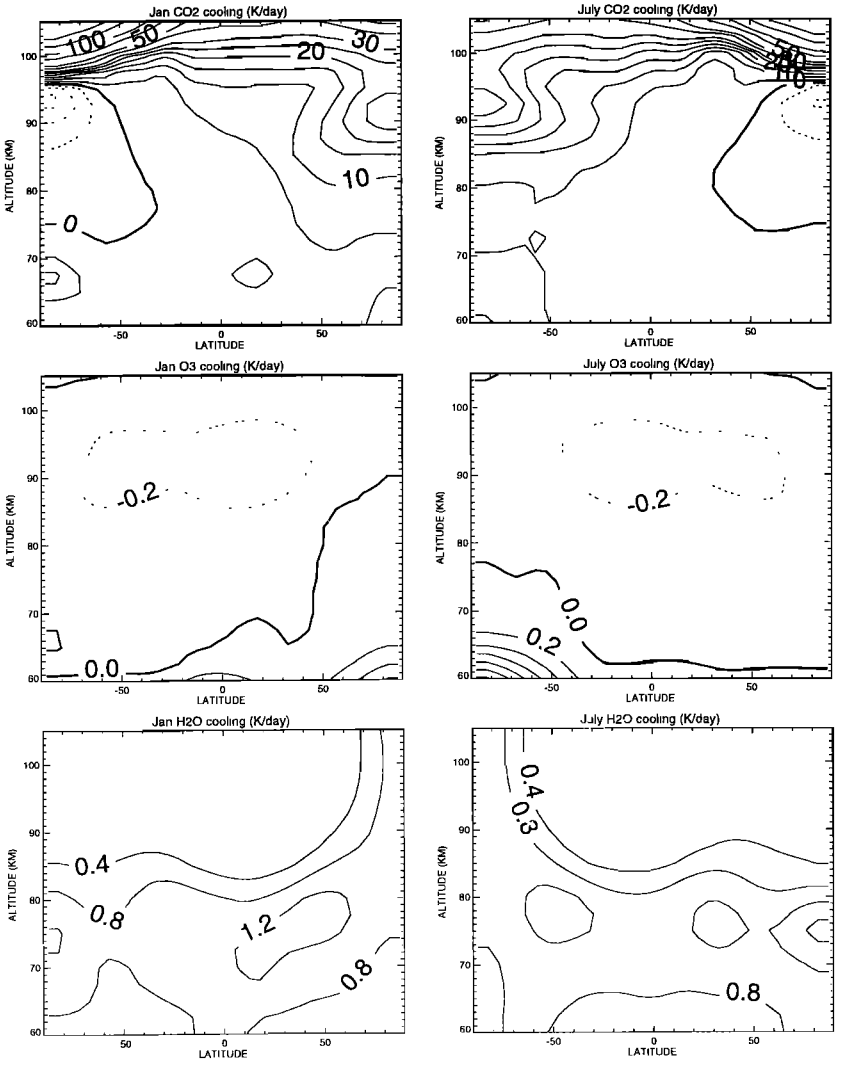

Figure 5. Cooling rates due to CO_2, O_3 and H_2O for (left) January and (right) July. Units are K d^{-1}.

molecular heat conduction rate cannot be made. Instead, the correction factor in (2) accounts for this process, as well as for errors in the other contributions to the net heating. The net heating rate adjusted to yield a zero global mean diabatic heating is shown in Figure 6.

The vertically divergent heat flux associated with dissipating diurnal tides $[\rho_0^{-1}(\rho_0\overline{w'\theta'})_z]$ may significantly affect the zonally averaged thermal budget [*Miyahara,* 1984; *Miyahara and Wu,* 1989]. Computation of this term requires estimates of diurnal temperature and vertical wind during the time periods under consideration. The diurnal wind can be readily analyzed in HRDI meridional winds [*Hays et al.,* 1994; *Khattatov et al.,* 1996]; however, extraction of diurnal zonal wind and temperature is more difficult owing to rapid temporal and vertical variations in HRDI time-mean temperatures and winds [*Lieberman and Hays,* 1994; *Forbes et al.,* 1997]. We therefore quantify this term by using classical theory to derive (1,1) vertical winds and temperature from monthly mean HRDI diurnal meridional winds. *Lieberman and Hays* [1994] and *Lieberman* [1997] have demonstrated that the classical approach yields (1,1) estimates that are consistent with the more accurate, highly tuned model determinations of *Khattatov et al.* [1997] and *Yudin et al.* [1997] at the equator. The derivation of the (1,1) vertical wind from the observed meridional wind is discussed extensively by *Lieberman and Hays* [1994], and the details will not be reiterated here. The temperature perturbation is obtained in a similar manner to the vertical wind, namely, by applying the relationship between temperature and the scaled vertical velocity variable y in the classical tidal framework [*Chapman and Lindzen,* 1970, p. 112].

Figure 7 shows a latitude-time section of monthly mean diurnal $\rho_0^{-1}(\rho_0\overline{w'\theta'})_z$ at 100 km, the altitude at which this quantity maximizes in the HRDI data. Tidal heating peaks at the equator, with secondary maxima at about 30°. Substantial seasonal and interannual variability is present in the tidal flux divergence, which track the variability of the diurnal tide itself [*Burrage et al.,*1995b; *Lieberman,*1997]. The strongest heating values are about 10 K d^{-1}, and occur during the equinoxes of 1992, 1993, and 1995. On the other

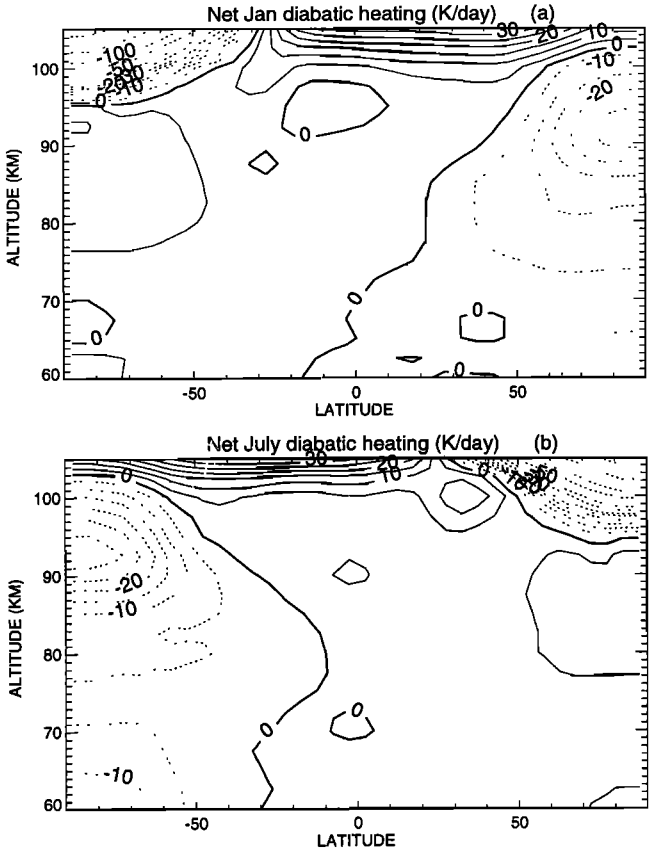

Figure 6. Net diabatic heating rates for (a) January and (b) July. Units are K d^{-1}.

hand, we note that the periods considered in the present study are characterized by the weakest values of tidal heating (under 1 K d^{-1}) between 1992–1995. A comparison between Figures 6 and 7 indicates that tidal heating at its strongest (~1 K d^{-1}) is at most 20–25% of the net radiative heating rate (~5 K d^{-1} in the tropics) in the immediate vicinity of 100 km. Above 100 km, tidal heating attenuates rapidly, while the net diabatic heating increases dramatically. While Figure 7 shows that the diurnal tides are a potentially significant source of wave heating in the lower thermosphere, we conclude that during the solstices of late 1993 and 1994, tidal heating above 100 km is insignificant compared with diabatic heating.

Adopting all of our simplifications reduces (1)–(3) to the following system:

$$\cos\phi^{-1}(\overline{v}^*_D \cos\phi)_y + \rho_0^{-1}(\rho_0 \overline{w}^*_D)_z = 0 \quad (6)$$

$$\overline{v}^*_D \overline{\Theta}_y + \overline{w}^*_D \overline{\Theta}_z =$$

$$e^{\kappa z/H}(\overline{Q}_r + \sigma) + \overline{Q}_{chem} \quad (7)$$

$$\int_{-\pi/2}^{\pi/2} \rho \overline{w}^*_D \cos\phi d\phi = 0. \quad (8)$$

Here $\overline{v}^*_D$ and $\overline{w}^*_D$ now denote the diabatic meridional and vertical wind, so named because the residual circulation is now proportional only to the time-averaged rate of the diabatic heating [*Holton*, 1992]. When the radiative and chemical terms on the right-hand side of (7) are specified, (6)–(8) can be solved iteratively for $\overline{v}^*_D$ and $\overline{w}^*_D$. Following *Huang and Smith* [1991], $\overline{v}^*_D$ is set to zero for the first iteration; $\overline{w}^*_D$ then becomes a function of the unknown correction factor σ, and this expression is substituted into (8) to solve for σ. With σ known, $\overline{w}^*_D$ is determined from (7) and then used in (6) to obtain $\overline{v}^*_D$. The new values of $\overline{v}^*_D$ and $\overline{w}^*_D$ are used in (7) to start the iteration anew, continuing until $\overline{v}^*_D$, $\overline{w}^*_D$ and σ converge (usually in under 10 iterations). Heating inputs and wind output fields are smoothed with a five-point running mean in latitude before plotting.

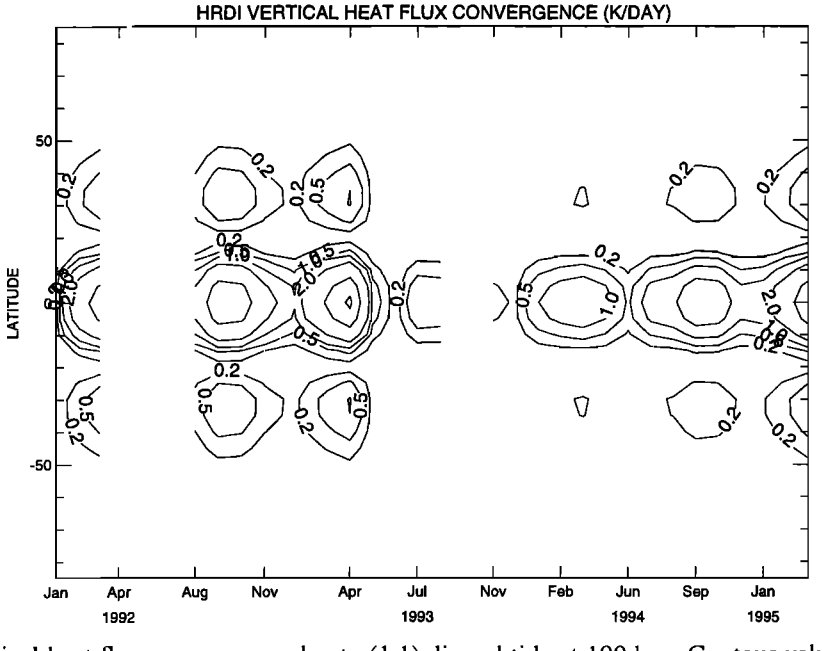

Figure 7. Vertical heat flux convergence due to (1,1) diurnal tide at 100 km. Contour values are ± 0.2, 0.5, 1, 2, 5, and 8 K d^{-1}.

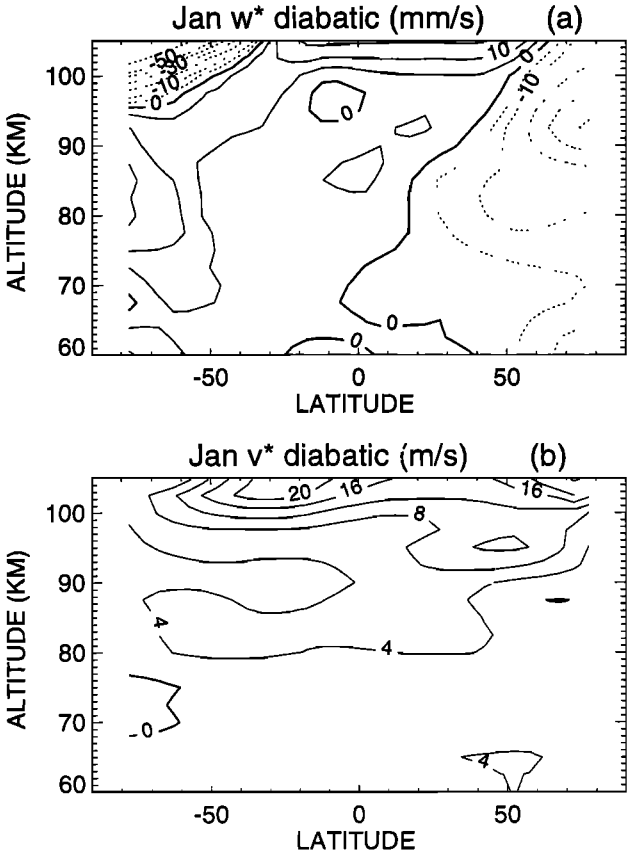

Figure 8. (a) January diabatic vertical wind, in mm s^{-1}. (b) Diabatic meridional wind, in m s^{-1}.

3. Diabatic and Observed Meridional Winds

The circulation required to balance the net diabatic heating rates shown in Figure 6 is plotted in Figures 8 and 9. The diabatic vertical wind generally echoes the heating rate, with ascent (descent) in regions of heating (cooling). The weak static stability within the cold summer mesopause results in an ascent rate that is quite strong, despite the relatively weak heating. The meridional wind is directed from the summer to winter hemisphere throughout most of the MLT. Peak values exceed 20 m s^{-1} and are found in the summer hemisphere near 25° and 105 km. A local maximum also appears at about 50° in the winter hemisphere, near 95 km, which is more pronounced in the southern Hemisphere (July).

For the June–August 1994 case, the diabatic circulation extends farther downward, with significant summer-to-winter pole flow at altitudes as low as 60 km. A broad secondary maximum in the diabatic meridional wind appears in the winter, or southern, Hemisphere between 70 and 80 km (Figure 9b). This feature is absent for the December–February case. Downward extension of the solstice diabatic circulation into the lower winter mesosphere was reported by *Huang and Smith* [1991], who associated this with stationary planetary wave driving. *Smith* [1996; 1997] has identified persistent, planetary-scale zonal asymmetries in HRDI mesospheric winds during February and August. Evidence for forced, vertically propagating waves that can drive $\overline{v}^*$ was found only during southern Hemisphere winter conditions (August). During northern Hemisphere winter (February), vertically propagating planetary waves did not penetrate higher than the lower mesosphere (about 60 km). Thus the weaker values of wintertime $\overline{v}^*_D$ in the lower mesosphere during January–February may be related to the absence of vertically propagating planetary waves.

Diabatic meridional winds are compared with zonally averaged or Eulerian mean HRDI meridional winds near 95 km. HRDI senses nighttime emission from a thin layer of chemiluminescence, which migrates between 92 and 97 km [*Burrage et al.*, 1994]. HRDI nighttime winds are generally associated with 95 km and are reported at this level along with daytime winds. The availability of HRDI nighttime and daytime wind retrievals implies nearly 24 hours of local time coverage and, in theory, the potential to separate the time-mean and the tidal components of the HRDI wind. The mean standard deviation of the HRDI daytime winds used in this study is about 7 m s^{-1}. Owing to the lower signal-to-noise ratio of the nighttime emissions, the uncertainty of the nighttime winds is about 13 m s^{-1}. Nighttime and daytime winds are weighted evenly in the determination of the 24-hour mean, yielding an uncertainty of approximately 6 m s^{-1} [*Ghil et al.*, 1981].

Lieberman et al. [1998] examined 60–day averages of HRDI 95-km meridional winds for six solstice-centered periods. Their values for the December 1993 to February 1994 and June–July 1994 cases are compared in Figures 10

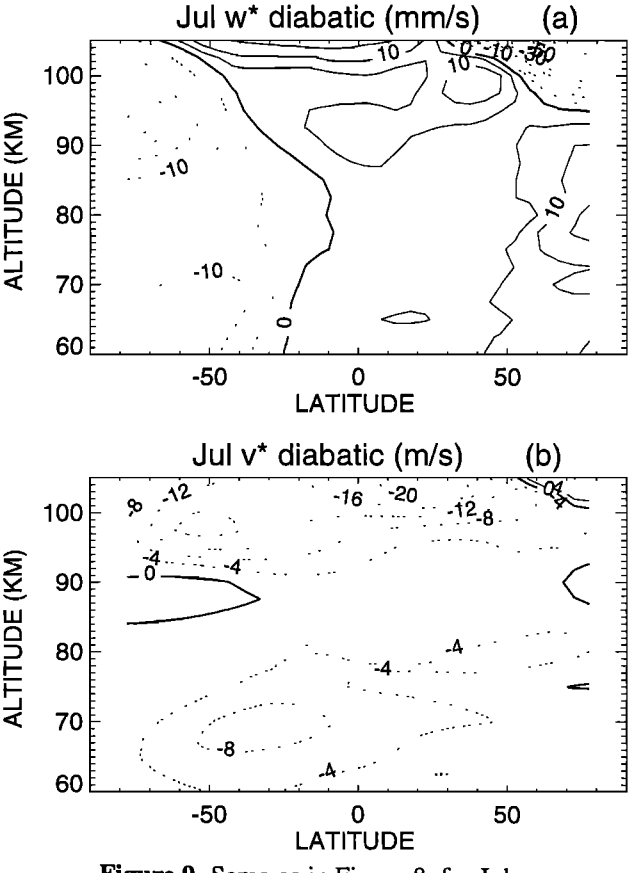

Figure 9. Same as in Figure 8, for July.

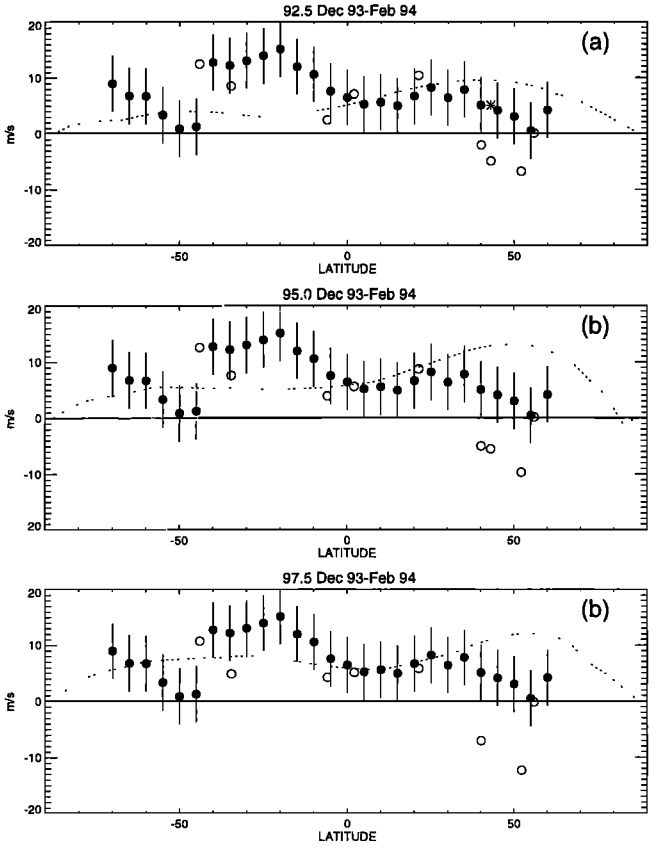

Figure 10. Dashed lines indicate January diabatioc meridional winds. Open circles indicate radar meridional winds, averaged between December 11, 1993, and February 9, 1994. Meteor wind value at Londonis indicated by asterisk. Solid circles indicate HRDI 95-km meridional winds, averaged between December 11, 1993, and February 9, 1994. Shown are (a) 92.5 km, (b) 95 km, and (c) 97.5 km.

and 11 with residual winds at 92.5, 95, and 97.5 km. It should be noted that in these figures, there is an exact correspondence between the periods examined by *Lieberman et al.* [1998] and the HRDI temperatures used to compute the diabatic winds. The directionality of the diabatic winds is consistent with HRDI Eulerian winds, with both fields indicating flow from the summer toward the winter hemisphere between 50°S and 50°N. HRDI winds peak in the low-latitude summer hemisphere, with values that are significantly stronger than the corresponding diabatic winds. A sharp decrease in HRDI wind magnitudes is seen near 50° in the summer hemisphere, with values increasing again poleward. This behavior is not seen in the residual wind field. Diabatic winds in the winter hemisphere are stronger than HRDI winds, particularly at 95 and 97.5 km.

Radar meridional winds are available for comparison with residual winds at the following locations: Christchurch, New Zealand (44°S,173°E); Adelaide, Australia (35°S,138°E); Jakarta, Indonesia (6°S,107°E); Christmas Island (2°N,157°W); Kauai, Hawaii (22°N,160°W); Urbana, Illinois (40°N,88°W); London, Canada (43°N,81°W); Saskatoon, Canada (52°N,107°W); and Kazan Russia (56°N, 49°E). Kazan, Jakarta and London are meteor wind (MW) systems. The remaining sites, including London, are MF or partial reflection radars. The instrumentation and measurement techniques are described fully in the references cited by *Lieberman et al.* [1998]. Briefly, the MF technique determines the horizontal drift velocity of weakly ionized irregularities that partially reflect incident radio waves from the 60- to 100-km height range. At heights below 100 km, where neutral ion collisions are large, these are assumed to represent the neutral wind. MW radars detect ionized meteor trail echoes that are also assumed, under quiet electric field conditions, to move with the neutral wind. There have been several recent and largely satisfactory comparisons between MF radars and ground- and space-based optical systems [*Cervara and Reid,* 1995; *Manson et al.,* 1996; *Burrage et al.,* 1996a; *Meek et al.,* 1997]. While wind directions and phases are generally in agreement between systems, most of these comparisons show modest but significant speed biases (0–50%) for the MF systems.

Figures 12 and 13 show radar meridional winds averaged between December 11, 1993 and February 9, 1994, and between June 13 and August 12, 1994. Diabatic winds and HRDI 95-km mean meridional winds are also plotted. During December–February, all three wind fields agree with respect to direction above 85 km in the southern Hemisphere and in the winter hemisphere as far north as Hawaii. At lat-

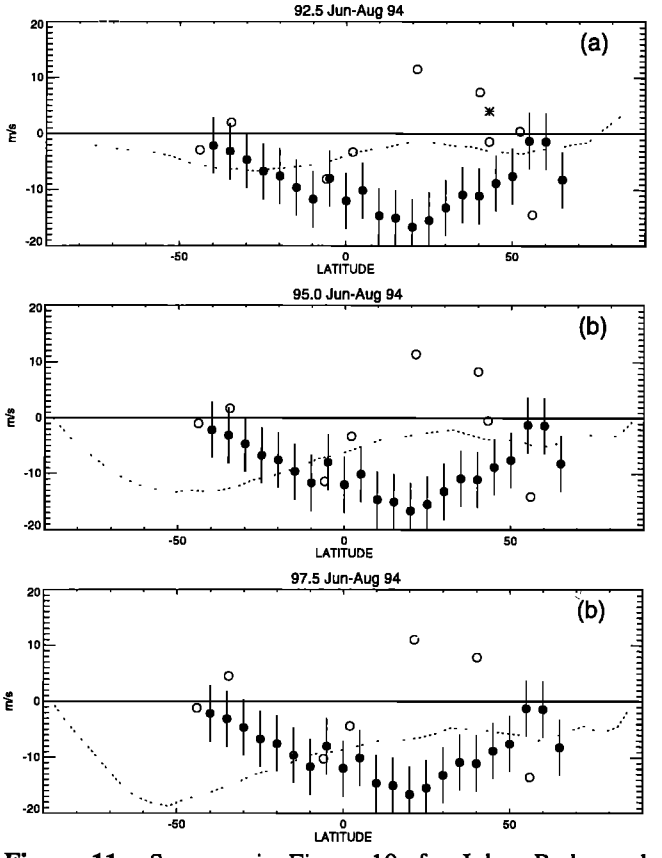

Figure 11. Same as in Figure 10, for July. Radar and HRDI 95-km winds averaged between June 13 and August 12, 1994.

itudes farther north, MF radar winds above 90 km are directed opposite to diabatic winds and to HRDI winds. At London, the MW winds are directed opposite to the MF winds and are in excellent agreement with HRDI and diabatic winds as a result. For the June–August case, consistency between the three wind field directions is greatest at the equatorial locations (Jakarta and Christmas Island), Saskatoon, and for the London MF winds. In the winter latitudes (Adelaide and Christchurch), radar winds are similar to HRDI winds and are close to zero. Both differ from the diabatic winds. Summertime radar winds at Kazan are in the same direction as HRDI and diabatic mean winds, but are considerably stronger.

4. Discussion and Summary

The diabatic circulation is computed with HRDI seasonally averaged solstice MLT temperatures. Meridional winds are directed from the summer to the winter hemisphere throughout the MLT. Peak values are between 20 and mbox25 m s^{-1}, observed at 105 km near 20° in the summer hemisphere. Comparisons with HRDI Eulerian mean winds near 95 km indicate that the two wind fields are of the same sign throughout most of the two summer hemispheres, although HRDI winds are stronger between 10° and 50°. Eulerian winds are weaker than diabatic winds in both midlatitude winter hemispheres. The HRDI Eulerian meridional wind agrees qualitatively with seasonally averaged radar winds between 50°S and 22°N during Southern Hemisphere summer, and between 50°S and 2°N during Northern Hemisphere summer. The largest disagreements between HRDI winds and MF radars occur in the Northern Hemisphere, in both winter (40°–55°N) and summer (20°–40°N). The direction differences between MF and MW winds at London seem to occur seasonally (in wintertime) and not regularly, (W. Hocking, personal communication, 1999), and this discrepancy is still under investigation. It has been suggested by *Hines et al.* [1993] that above 90 km, the MF technique measures the horizontal phase speed of gravity waves along with the background wind, thus rendering a depiction of the wind field that might differ from the meteor wind measurement. *Hocking* [1997] has also commented on the potential for contamination of MF winds above 90 km by E region scattering.

Residual and measured winds can differ for several reasons. Radar winds are point measurements taken at fixed altitudes. HRDI Eulerian mean winds are quantities that are zonally averaged on constant altitude surfaces. Residual winds approximate quantities that are zonally averaged with respect to a constant log-pressure surface. As noted in section 1, if stationary waves are present, then season-

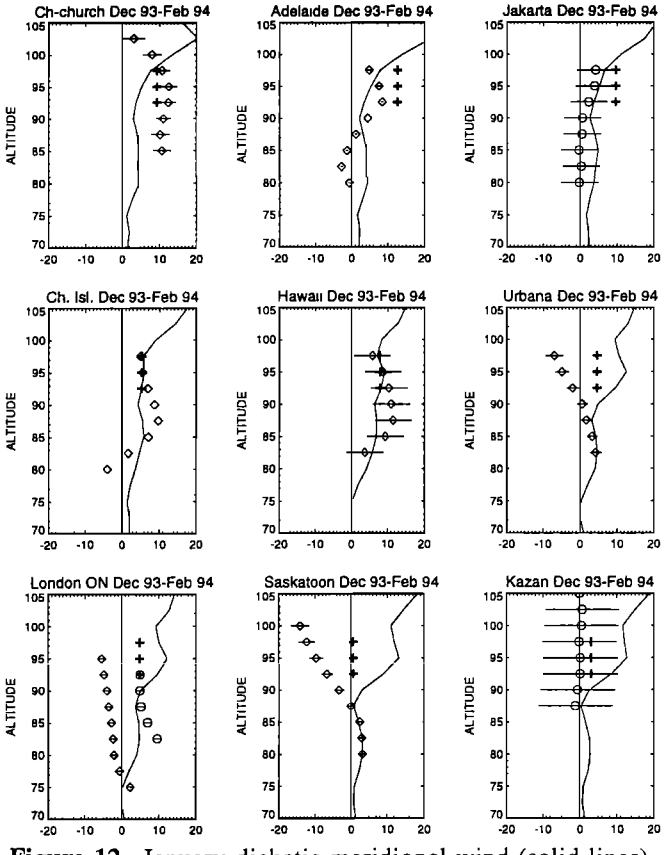

Figure 12. January diabatic meridional wind (solid lines), MF radar (diamonds) and MW (circles) meridional winds averaged between December 11, 1993, and February 9, 1994. HRDI 95-km mean meridional winds (averaged between December 11, 1993 and February 9, 1994 are shown for reference at 92.5, 95 and 97.5 km (plus signs).

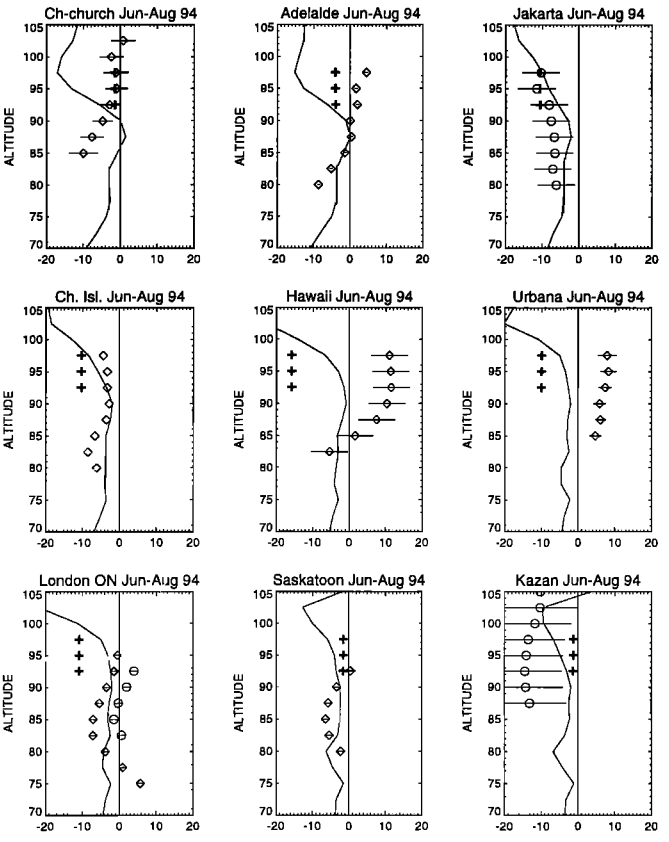

Figure 13. Same as in Figure 12, for July. Radar and HRDI 95-km winds averaged between June 13 and August 12, 1994.

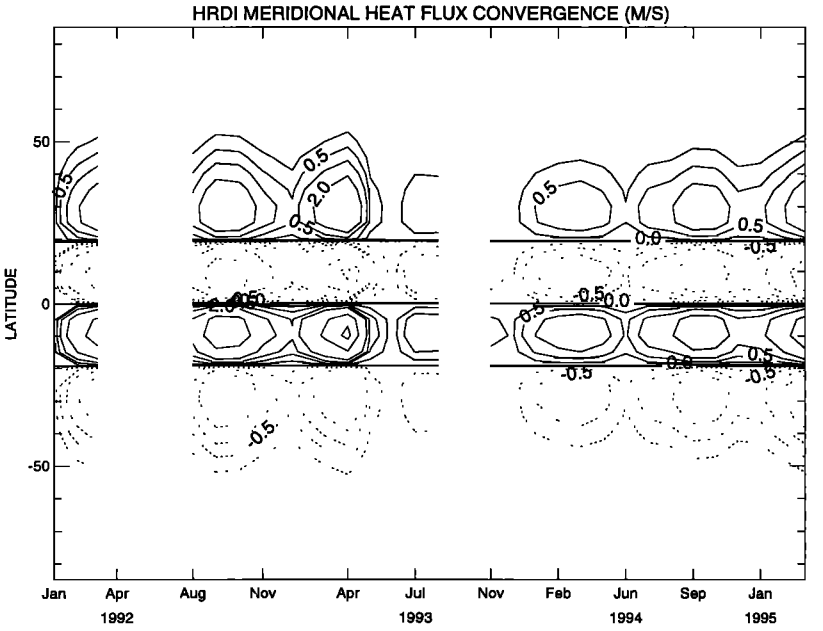

Figure 14. Meridional heat flux convergence due to (1,1) diurnal tide at 100 km. Contour values are ± 0.2, 0.5, 1, 2, 5, and 8 m s^{-1} d^{-1}.

ally averaged radar measurements approximate the Eulerian zonal mean about a constant altitude, plus the wave contribution. The findings of *Smith* [1997] indicate that stationary planetary waves are present in the Northern and Southern Hemisphere wintertime MLT. These may account for the significant differences between MF radar and zonally averaged winds at these times.

Differences between HRDI and residual mean winds may be interpreted in terms of planetary wave driving effects. HRDI provides an estimate of the Eulerian mean meridional wind, which differs from the residual (or diabatic) wind if vertically divergent planetary-scale wave heat fluxes of significant magnitudes are present (see equation (4)). These are generally associated with vertically propagating stationary planetary waves. *Smith* [1997] analyzed HRDI MLT winds and found evidence for wintertime vertical propagation in the Southern (but not the Northern) Hemisphere. These findings suggest the possibility that stationary planetary waves may drive residual meridional winds away from Eulerian winds in the Southern Hemisphere wintertime MLT.

The 2–day wave is a ubiquitous feature of the summertime MLT [*Harris*, 1994] that has the potential to drive the mean flow by virtue of its transient and dissipative behavior [*Pfister*, 1985; *Plumb et al.*, 1987; *Fritts et al.*, 1999]. *Lieberman* [1999a] estimated the Eulerian and residual meridional winds induced by an unstable 2–day wave event in January 1994. The two fields were directed opposite to each other but were considerably weaker (less than 1 m s^{-1}) than the theoretical and observed meridional winds reported here. Meridional heat convergence due to the diurnal tide could also account for differences between Eulerian and residual mean flows. Figure 14 shows a latitude-time section of diurnal meridional heat flux convergence at 100 km, computed in a manner similar to Figure 7. As seen with the vertical heat flux divergence, tidal dissipation is capable of generating significant meridional heat flux divergence; however, this term is quite weak for the periods we are considering.

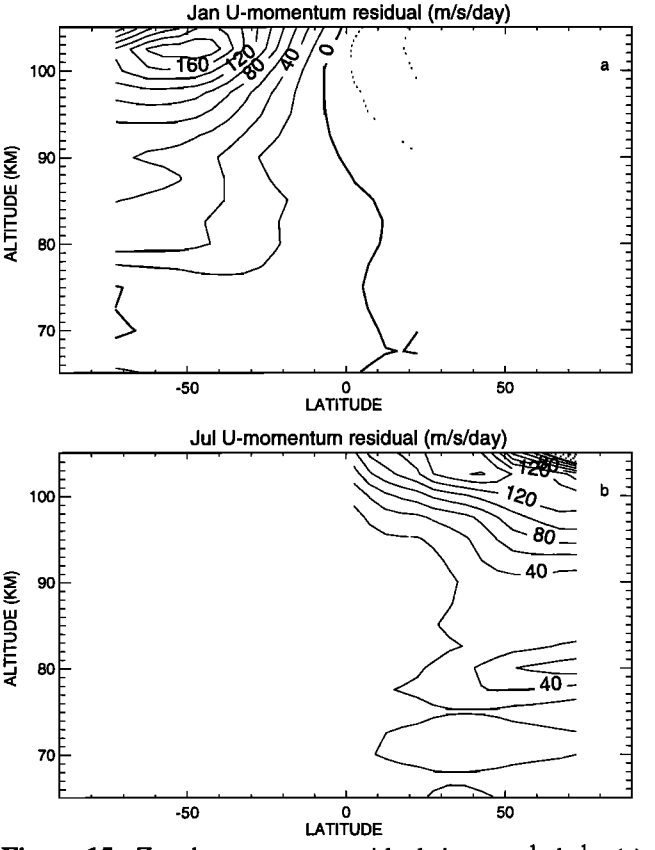

Figure 15. Zonal momentum residual, in m s^{-1} d^{-1}. (a) January. (b) July.

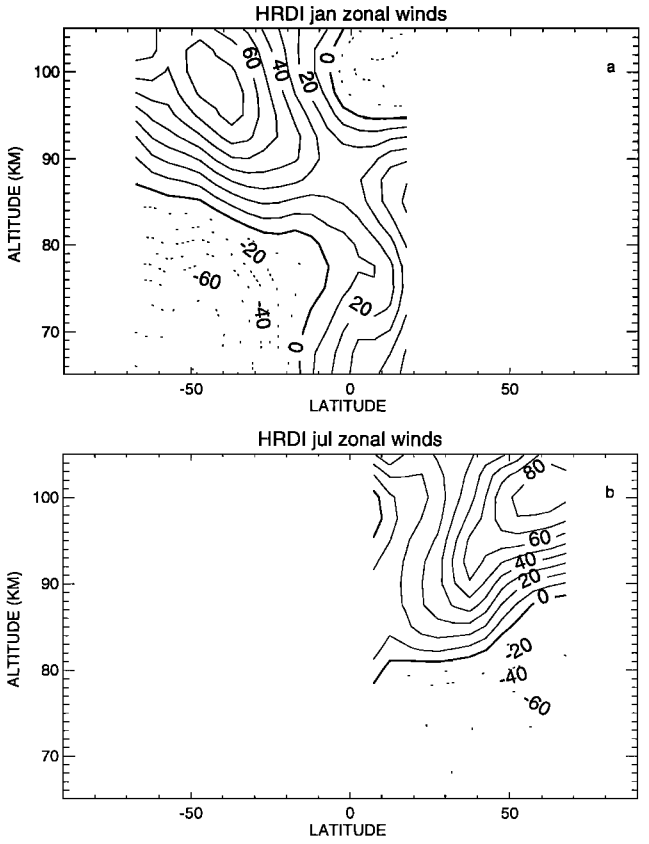

Figure 16. HRDI zonal mean zonal wind. Contour interval is 10 m s^{-1}, and dotted contours indicate westward flow. (a) December 11, 1993, to February 9, 1994. (b) June 13 to August 12, 1994.

The diabatic winds presented in this study are stronger than those reported by *Huang and Smith* [1991], whose circulation was based upon the CIRA-86 temperature climatology. More recent modeling efforts by *Portmann* [1994] and *Zhu et al.* [1997] have produced residual meridional winds whose magnitudes are more consistent with our diabatic winds. The Portmann model is an updated version of the *Garcia and Solomon* [1985] model with improved radiative heating. Residual meridional winds peak at about 20 m s^{-1} in the summer hemisphere near 20°; however, the maximum occurs between 85 and 90 km, about 15 km lower than the corresponding maximum seen in Figures 8b and 9b.

Zhu et al. [1997] applied the *Zhu* [1994] radiative heating together with Lindzen-type gravity wave drag parameterizations in a model of the residual circulation. Their meridional wind maxima are of the order of 20–25 m s^{-1}, which are more consistent with HRDI 95-km mean meridional winds. The *Zhu et al.* [1997] winds peak near 95 km, about 10 km lower than the residual winds reported here. This may be because Zhu et al. tuned their model to yield zonal mean temperatures that are consistent with the CIRA-86 climatology, rather than the HRDI temperatures used in our study. It is worth noting that the strong circulations obtained by *Zhu et al* [1997] were produced by increasing the magnitude of the parameterized gravity wave drag to values as high as 400 m s^{-1} d^{-1}, substantially higher than previously used values.

Figure 15 shows the zonal mean momentum residual F, computed as

$$f\overline{v}^* - \cos\phi^{-1}(\overline{U}\cos\phi)_y\overline{v}^* + \overline{w}^*\overline{U}_z = F. \quad (9)$$

The zonal mean wind values used to compute F are HRDI winds averaged identically to the temperatures shown in Figure 3; these are shown in Figure 16. The bulk of F is due to the Coriolis torque upon $\overline{v}^*$. The momentum residual is westward in the summer hemisphere and peaks near 103 km between 150 and 200 m s^{-1} d^{-1}. These values are weaker than those imposed by *Zhu et al.* [1997], but stronger than momentum residuals implied by *Huang and Smith* [1991] or specified by *Garcia and Solomon* [1985] at solstice. A region of prominent eastward driving (about 60–70 m s^{-1} d^{-1}) appears in the Northern Hemisphere lower mesosphere during summer (July), which has no Southern Hemisphere summer (January) counterpart. This feature is associated with the lower mesospheric $\overline{v}^*$ noted in Figure 9.

Forcing of the MLT is ascribed largely to gravity waves, particularly during the summertime. Our results imply fairly vigorous wave driving in the the upper mesosphere and lower thermosphere, which maximizes at higher altitudes (above 100 km) than are reported or parameterized. A substantial momentum residual is also seen in the Northern Hemisphere lower mesosphere during June-August. In addition to the gravity wave drag assumed to dominate the MLT, evidence has been presented here for tidal driving and elsewhere for stationary propagating waves in the wintertime MLT [*Smith*, 1996;1997] and for 2-day wave-driving in the midlatitude summer MLT [*Lieberman*, 1999a]. The MLT diabatic winds presented in this study likely reflect the joint effects of planetary as well as gravity wave driving.

Further clarification of the MLT zonal momentum budget is needed, which requires several additional elements. The MLT zonally averaged temperature should contain minimal tidal contamination when used as input to the time-mean radiative heating. Achieving globally averaged heating and mass balance requires a more detailed specification of thermospheric heat inputs to the MLT than the latitude-independent correction employed in the present model. The effects of gravity waves upon the global-scale mean thermal budget may be more significant than suggested by the one-dimensional model of *Gavrilov and Roble* [1994] or the tuning studies of *Huang and Smith* [1991].

Acknowledgments. R. S. L. wishes to thank Xun Zhu and Theresa Y. W. Huang for helpful discussions about the numerical model. Additional thanks are due Dennis Riggin and Robert Stockwell for help in interpreting radar measurement uncertainties. We thank our anonymous reviewers for their insigntful comments and suggested improvements to the manuscript. This work was supported under NSF grant ATM-9812271.

References

Andrews, D. G., J. R. Holton, and C. B. Leovy, *Middle Atmosphere Dynamics*, Academic, San Diego, Calif., 1987.

Banks, P. M. and G. Kocharts, *Aeronomy*, Academic, San Diego, Calif., 1973.

Brasseur, G. and D. Offerman, Recombination of atomic oxygen near the mesopause: Interpretation of rocket data, *J. Geophys. Res., 91,* 10,818–10,824, 1986.

Brasseur, G., et al., An interactive chemical dynamical radiative two-dimensional model of the middle atmosphere, *J. Geophys. Res., 95,* 5639–5655, 1990.

Burrage, M. D., N. Arvin, W. R. Skinner, and P. B. Hays, Observations of the O_2 atmospheric band nightglow by the High Resolution Doppler Imager, *J. Geophys. Res., 99,* 15,017–15,023, 1994.

Burrage, M. D., M. E. Hagan, W. R. Skinner, D. L. Wu, and P. B. Hays, Long-term variability in the solar diurnal tide observed by HRDI and simulated by the GSWM, *Geophys. Res. Lett., 22,* 2641–2644, 1995.

Burrage, M. D. et al., Validation of mesospheric and lower thermospheric winds from the High Resolution Doppler Imager on UARS, *J. Geophys. Res., 101,* 10,365–10,392, 1996.

Cervera, M. A. and I. M. Reid, Comparison of simultaneous wind measurements using colocated VHF meteor radar and MF spaced antenna radar systems, *Radio Sci., 30,* 1245–1261, 1995.

Chapman, S., and R. S. Lindzen, *Atmospheric Tides,* D. Reidel, Norwell, Mass., 1970.

Coy, L. and D. C. Fritts, Gravity wave heat fluxes: A Lagrangian approach, *J. Atmos. Sci., 45,* 1770–1780, 1988.

Dickinson, R. E., Infrared cooling in the mesosphere and lower thermosphere, *J. Atmos. Terr. Phys., 46,* 995–1008, 1984.

Dunkerton, T. J., On the mean meridional mass motions of the stratosphere and mesosphere, *J. Atmos. Sci., 35,* 2325–2333, 1978.

Forbes, J. M., M. Kilpatrick, D. Fritts, A. H. Manson, and R. A. Vincent, Zonal mean and tidal dynamics from space: An empirical examination of aliasing and sampling issues, *Ann. Geophys., 15,* 1158–1164, 1997.

Fritts, D. C. and T. J. Dunkerton, Fluxes of heat and constituents due to convectively unstable waves, *J. Atmos. Sci., 42,* 549–556, 1985.

Fritts, D. C., et al., Two-day wave structure and mean-flow interactions observed by radar and HRDI, *J. Geophys. Res., 104,* 3953–3969, 1999.

Garcia, R. R., On the mean meridional circulation of the middle atmosphere, *J. Atmos. Sci., 44,* 3599–3609, 1987.

Garcia, R. R., and S. Solomon, The effect of breaking gravity waves on the dynamics and chemical composition of the mesosphere and lower thermosphere, *J. Geophys. Res., 90,* 3850–3868, 1985.

Gardner, C. S., and W. Yang, Measurement of the dynamical cooling rate associated with the vertical transport of heat by dissipating gravity waves at the Starfire Optical Range, New Mexico, *J. Geophys. Res., 103,* 16,909–16,926, 1998.

Gavrilov, N. M., and R. G. Roble, The effect of gravity waves on the global mean temperature and composition structure of the upper atmosphere, *J. Geophys. Res., 99,* 25,773–25,780, 1994.

Ghil, M., S. Cohn, J. Tavantzis, K. Bube, and E. Isaacson, Applications of estimation theory to numerical weather prediction, in *Dynamic Meteorology: Data Assimilation Methods*, edited by L. Bengtsson, M. Ghil, and E. Kellen, pp. 139–224, Springer-Verlag, New York, 1981.

Harris, T. J., A long-term study of the quasi-two-day wave in the middle atmosphere, *J. Atmos. Terr. Phys., 56,* 569–579, 1994.

Hays, P. B. et al., Observations of the diurnal tide from space, *J. Atmos. Sci., 51,* 3077–3093, 1994.

Hines, C. O., et al., Multi-instrument observations of mesospheric motions over Arecibo: Comparisons and interpretations, *J. Atmos. Terr. Phys., 55,* 241–287, 1993.

Hitchman, M. H. and C. B. Leovy, Diurnal tide in the equatorial middle atmosphere as seen in LIMS temperatures, *J. Atmos. Sci., 42,* 557–561, 1985.

Hitchman, M. H. and C. B. Leovy, Evolution of the zonal mean state in the equatorial middle atmosphere during October 1978–May 1979, *J. Atmos. Sci., 43,* 3159–3176, 1986.

Hocking, W. K., Strengths and limitations of MST radar measurements of middle-atmosphere winds, *Ann. Geophys., 15,* 1111–1122, 1997.

Holton, J. R., *An Introduction to Dynamic Meteorology,* Academic, San Diego, Calif., 1992.

Huang, T. Y. W., and A. K. Smith, The mesospheric diabatic circulation and the paramterized thermal effect of gravity wave breaking on the circulation, *J. Atmos. Sci., 48,* 1093–1111, 1991.

Keating, G. M., and M. C. Pitts, Proposed reference models for ozone, *Adv. Space Res., 7,* 937–947, 1987.

Khattatov, B. V., et al., Dynamics of the mesosphere and lower thermosphere as seen by radars and by the high-resolution Doppler imager/UARS, *J. Geophys. Res., 101,* 10,393–10,404, 1996.

Khattatov, B. V., M. A. Geller, V. A. Yudin, P. B. Hays, and R. A. Vincent, Diurnal migrating tide as seen by HRDI/UARS, 1: Monthly mean global meridional winds, *J. Geophys. Res., 102,* 4405–4422, 1997.

Leblanc, T., et al., Temperature climatology of the middle atmosphere from long-term lidar measurements at middle and lower latitudes, *J. Geophys. Res., 103,* 17,191–17,204, 1998.

Leovy, C. B., Simple models of thermally driven mesospheric circulations, *J. Atmos. Sci., 21,* 327–341, 1964.

Lieberman, R. S., Long-term variation of zonal mean winds and (1,1) driving in the equatorial lower thermosphere, *J. Atmos. Sol. Terr. Phys., 59,* 1483–1490, 1997.

Lieberman, R. S., Eliassen-Palm fluxes of the two-day wave, *J. Atmos. Sci., 56,* 2846–2861, 1999a.

Lieberman, R. S., The gradient wind in the mesosphere and lower thermosphere, *Earth Planets Space, 51,* 751–761, 1999b.

Lieberman, R. S., and P. B. Hays, An estimate of the momentum deposition in the lower thermosphere by the observed diurnal tide, *J. Atmos. Sci., 51,* 3094–3105, 1994.

Lieberman, R. S., et al., HRDI observations of mean meridional winds at solstice, *J. Atmos. Sci., 55,* 1887–1896, 1998.

Liu, H. L., Temperature changes due to gravity wave saturation, *J. Geophys. Res.,* in press, 2000.

Manson, A. H., et al., Comparisons between satellite-derived gradient winds and radar-derived winds from the CIRA-86, *J. Atmos. Sci., 48,* 411–428, 1991.

Manson, A. H., F. Yi, and C. E. Meek, Comparisons between instantaneous wind measurements made at Saskatoon (52°N,107°W) using colocated medium frequency radars and Fabry-Perot interferomter instruments: Climatologies (1988–1992) and case studies, *J. Geophys. Res., 101,* 29,553–29,563, 1996.

Meek, C. E., A. H. Manson, M. D. Burrage, G. Garbe, and L. L. Cogger, Comparisons between Canadian prairie MF radars, FPI (green and OH lines) and UARS HRDI systems, *Ann. Geophys., 15,* 1099–1110, 1997.

Miyahara, S., Zonal mean winds induced by solar diurnal tides in the lower thermosphere for a solstice condition, *Dynamics of the middle atmosphere,* edited by J. R. Holton and T. Matsuno, pp. 181–197, D. Reidel, Dordrecht-Holland, 1984.

Miyahara, S., and D. H. Wu, Effects of solar tides on the zonal mean circulation in the lower thermosphere: Solstice condition, *J. Atmos. Terr. Phys., 51,* 635–647, 1989.

Morton, Y. T., et al., Global mesospheric tidal winds observed by the High Resolution Doppler Imager on board the Upper Atmosphere Research Satellite, *Geophys. Res. Lett., 20,* 1263–1266, 1993.

Ortland, D. A., P. B. Hays, W. R. Skinner, and J. H. Yee, Remote sensing of mesospheric temperature and $O_2(^1\Sigma)$ band volume

emission rates with the High Resolution Doppler Imager, *J. Geophys. Res., 103*, 1821–1835, 1998.

Pfister, L., Baroclinic instability of easterly jets with applications to the summer mesosphere, *J. Atmos. Sci., 42*, 313–330, 1985.

Plumb, R. A., R. A. Vincent, and R. L. Craig, The quasi-2-day wave event of January 1984 and its impact on the mean mesospheric circulation, *J. Atmos. Sci., 44*, 3030–3036, 1987.

Portmann, R. W., The heat budget and global change in the mesosphere, Ph.D. thesis, 187 pp., Dept. of Astrophys. Planet. and Atmos. Sci., Univ. of Colo., Boulder, 1994.

Schoeberl, M. R., D. F. Strobel, and J. P. Apruzese, A numerical model of gravity wave breaking and stress in the mesosphere, *J. Geophys. Res., 88*, 5249–5259, 1983.

Shine, K., Sources and sinks of zonal momentum in the middle atmosphere diagnosed using the diabatic circulation, *Q. J. R. Meteorol. Soc., 115*, 265–292, 1989.

Smith, A. K., Longitudinal variations in mesospheric winds: Evidence for gravity wave filtering by planetary waves, *J. Atmos. Sci., 53*, 1156–1173, 1996.

Smith, A. K., Stationary planetary waves in upper mesospheric winds, *J. Atmos. Sci., 54*, 2129–2145, 1997.

Solomon, S., J. T. Kiehl, R. R. Garcia, and W. Grose, Tracer transport by the diabatic circulation deduced from satellite observations, *J. Atmos. Sci., 43*, 1603–1617, 1986.

Strobel, D. F., Parameterization of the atmospheric heating rate from 15 to 120 km due to O_2 and O_3 absorption of solar radiation, *J. Geophys. Res., 83*, 6225–6230, 1978.

Strobel, D. F., Constraints on gravity wave induced diffusion in the middle atmosphere, *Pure Appl. Geophys., 130*, 533–546, 1989.

Strobel, D. F., J. P. Apruzese, and M. R. Schoeberl, Energy balance constraints on gravity wave induced eddy diffusion in the mesosphere and lower thermosphere, *J. Geophys. Res., 90*, 13,067–13,072, 1985.

Yudin, V. A. et al., Thermal tides and studies to tune the mechanistic tidal model using UARS observations, *Ann. Geophys., 15*, 1205–1220, 1997.

Zhu, X., Carbon dioxide 15-μ band cooling rates in the upper atmosphere calculated by Curtis matrix interpolation, *J. Atmos. Sci., 47*, 755–774, 1990.

Zhu, X., An accurate and efficient radiation algorithm for middle atmosphere models, *J. Atmos. Sci., 51*, 3593–3614, 1994.

Zhu, X., P. K. Swaminathan, J. H. Yee, D. F. Strobel, and D. Anderson, A globally balanced two-dimensional middle atmosphere model: Dynamical studies of mesopuase meridional circulation and stratosphere-mesosphere exchange, *J. Geophys. Res., 102*, 13,095–13,112, 1997.

A. Fahrutdinova, Physics Department, Kazan State University, 18 Lenin St., Kazan, 420008 Russia. (Antonina.Fahrutdinova@ksu.ru)

S. J. Franke, Department of Electrical and Computer Engineering, CSRL MC-229, 1308 W. Main Street, University of Illinois, Urbana, IL 61801. (sfranke@ece.uiuc.edu)

G. J. Fraser, Department of Physics and Astronomy, University of Canterbury, Private Bag 4800, Christchurch 8020, New Zealand. (phys041@cantva.canterbury.ac.nz)

W. Hocking and J. MacDougall, Department of Electrical Engineering, University of Western Ontario, 1155 Richmond St., London, Ontario, Canada. (macdougall@danlon.physics.uwo.ca, whocking@danlon.physics.uwo.ca).

J. R. Isler, Department of Physics, Wagner College, 631 Howard Ave., Staten Island, NY 10301.

R. S. Lieberman, Northwest Research Asssociates, Colorado Research Associates Division, 3380 Mitchell Lane, Boulder, CO 80301. (ruth@colorado-research.com)

A. H. Manson and C. E. Meek, Institute of Space and Atmospheric Studies, University of Saskatchewan, 116 Science Place, Saskatoon, Saskatchewan, Canada (manson@dansas.usask.ca)

T. Nakamura and T. Tsuda, Radio Atmospheric Science Center, Uji, Kyoto 611-0011, Japan. (nakamura@kurasc.kyoto-u.ac.jp)

A. K. Smith, Atmospheric Chemistry Division, National Center for Atmospheric Research, Boulder, CO 80307. (aksmith@aksmith.acd.ucar.edu)

T. Thayaparan, Defense Research Establishment Ottawa, 3701 Carling Ave., Ottawa, Ontario, Canada. (Thayananthan.Thayaparan@dreo.dnd.ca)

R. A. Vincent, Department of Physics and Mathematical Sciences, University of Adelaide, G.P.O. Box 498, Adelaide, S. Australia 5001. (rvincent@physics.adelaide.edu.au)

(Received August 24, 1999; revised May 26, 2000;
accepted May 31, 2000.)